

# Reionization optical depth determination from *Planck* HFI data with ten percent accuracy

L. Pagano<sup>1,2,3,4</sup> \*, J.-M. Delouis<sup>5,3,6</sup>, S. Mottet<sup>3,6</sup>, J.-L. Puget<sup>4,2,3</sup>, and L. Vibert<sup>2,3</sup>

<sup>1</sup> Dipartimento di Fisica e Scienze della Terra, Università degli Studi di Ferrara and INFN – Sezione di Ferrara, Via Saragat 1, 44122 Ferrara, Italy

<sup>2</sup> Institut d’Astrophysique Spatiale, CNRS, Univ. Paris-Sud, Université Paris-Saclay, Bât. 121, 91405 Orsay cedex, France

<sup>3</sup> Institut d’Astrophysique de Paris, CNRS (UMR7095), 98 bis Boulevard Arago, F-75014, Paris, France

<sup>4</sup> LERMA, Sorbonne Université, Observatoire de Paris, Université PSL, École normale supérieure, CNRS, Paris, France

<sup>5</sup> Laboratoire d’Océanographie Physique et Spatiale (LOPS), Univ. Brest, CNRS, Ifremer, IRD, Brest, France

<sup>6</sup> Sorbonne Université, UMR7095, 98 bis Boulevard Arago, F-75014, Paris, France

Wednesday 27<sup>th</sup> May, 2020

## ABSTRACT

We present an estimation of the reionization optical depth  $\tau$  from an improved analysis of the High Frequency Instrument (HFI) data of *Planck* satellite. By using an improved version of the HFI map-making code, we greatly reduce the residual large scale contamination affecting the data, characterized, but not fully removed, in the *Planck* 2018 legacy release. This brings the dipole distortion systematic effect, contaminating the very low multipoles, below the noise level. On large scale polarization only data, we measure  $\tau = 0.0566^{+0.0053}_{-0.0062}$  at 68% C.L., reducing the *Planck* 2018 legacy release uncertainty by  $\sim 40\%$ . Within the  $\Lambda$ CDM model, in combination with the *Planck* large scale temperature likelihood, and the high- $\ell$  temperature and polarization likelihood, we measure  $\tau = 0.059 \pm 0.006$  at 68% C.L. which corresponds to a mid-point reionization redshift of  $z_{re} = 8.14 \pm 0.61$  at 68% C.L.. This estimation of the reionization optical depth with 10% accuracy is the strongest constraint to date.

**Key words.** Cosmology: observations – dark ages

## 1. Introduction

Cosmological recombination around redshift  $z = 1100$  produces a mostly neutral universe, starting the so called Dark Ages. At later stages the Universe’s dark ages end with the formation of the first galaxies. The lack of Gunn-Peterson trough (Gunn & Peterson 1965; Scheuer 1965) in the spectra of distant quasars (Rauch 1998; Becker et al. 2001; Fan et al. 2006) revealed that the Universe had become almost fully reionized by redshift  $z \simeq 6$  (Dayal & Ferrara 2018).

In the context of cosmological observations, Cosmic Microwave Background (CMB) generated at recombination and propagating almost freely to us, is mostly influenced by the total amount of free electrons along the line of sight, parametrized by the Thomson scattering optical depth to reionization  $\tau$ , one of the six parameters of the  $\Lambda$ CDM model.

Reionization has mainly two effects on CMB power spectra. Firstly, it damps by a factor  $e^{-2\tau}$  scalar perturbations as generated at recombination. This makes the amplitude  $A_s$  of the scalar perturbation highly degenerate with  $\tau$  for high multipoles measurements. Secondly the re-scattering of the CMB photons on free electrons at the reionization epoch generates a bump on polarization power spectra at large angular scale. The position and height of this bump depend on the mean reionization redshift ( $z_{re}$ ) and on the duration of the reionization transition. The measured quantity on the spectra at high multipoles is  $A_s e^{-2\tau}$  and thus  $\delta A_s / A_s = 2\delta\tau$ . The measure of the large scale polarization allows to break the degeneracy with  $A_s$  and provides directly  $\tau$ . A ten percent relative accuracy on  $\tau$  correspond to a 1% accuracy on  $A_s$  if  $\tau$  is about 0.05. The direct measurement of  $\tau$  on the reionization peak is thus critical.

Although the reionization optical depth determination has been greatly improved in the last two decades,  $\tau$  is still the less constrained parameter of the  $\Lambda$ CDM model (Weiland et al. 2018; Planck Collaboration VI 2019). The reionization peak being visible only at very large scales ( $\ell < 10$ ) both in  $EE$  and  $TE$  spectra, it has been directly measured only on full sky polarized observations by space experiments. The first measurement from Wilkinson Microwave Anisotropy Probe (WMAP) (Kogut et al. 2003) gave  $\tau = 0.17 \pm 0.04$  based on  $TE$  spectrum, while on the final 9yr WMAP maps Hinshaw et al. (2013) reported  $\tau = 0.089 \pm 0.014$  measured on  $TE$  and  $EE$  spectra. *Planck* collaboration in a re-analysis of the WMAP maps (Planck Collaboration V 2019) used the *Planck* 353GHz map as dust tracer rather than the WMAP dust template (Page et al. 2007), based on the starlight-derived polarization directions and the Finkbeiner-Davis-Schlegel dust model (Finkbeiner et al. 1999), lowering  $\tau$  by roughly  $2\sigma$  to  $\tau = 0.062 \pm 0.012$ .

Using *Planck* only data and Low Frequency Instrument (hereafter LFI) 70 GHz (Planck Collaboration II 2019) map as main cosmological channel, *Planck* Collaboration found compatible values of  $\tau = 0.067 \pm 0.023$  in the 2015 release (Planck Collaboration XI 2016) and  $\tau = 0.063 \pm 0.020$  in the 2018 legacy release (Planck Collaboration V 2019). After the *Planck* 2015 release Lattanzi et al. (2017) reanalyzed all the available datasets and combined LFI 2015 data with WMAP finding  $\tau = 0.066^{+0.012}_{-0.013}$ .

All those results are obtained using the same general method, i.e. CMB maps are cleaned from foreground contamination and then the probability is directly computed on maps assuming Gaussian signal and noise (Tegmark 1996; Page et al. 2007; Lattanzi et al. 2017). This relies on accurate estimation of the noise bias covariance matrix. An exhaustive review of all the

\*Corresponding author: L. Pagano, luca.pagano@unife.it

measures before the *Planck* 2018 legacy release can be found in Weiland et al. (2018).

For the *Planck* HFI data, being more sensitive than WMAP and LFI channels, but then more vulnerable to systematic effects, a different approach was followed by the *Planck* Collaboration. In this case, given the difficulty of estimating reliable covariance matrices, a spectrum based likelihood was developed, acting on the cross-spectrum of 100 and 143 GHz maps. Following this approach, *Planck Collaboration Int. XLVI* (2016) measured  $\tau = 0.055 \pm 0.009$  in an intermediate analysis of HFI data after the *Planck* 2015 release, while  $\tau = 0.051 \pm 0.009$  is reported in the *Planck* 2018 legacy release (*Planck Collaboration V* 2019).<sup>1</sup> Overall, still the major limitation is the presence of large scale systematic effects, highly reduced with respect to *Planck* 2015 analysis but not brought below the noise level.

For a clearer global picture we report the main  $\tau$  constraints to date, in the base  $\Lambda$ CDM model, for different large scale CMB datasets:

$$\begin{aligned} \tau &= 0.089 \pm 0.013 \text{ Ka, Q and V with WMAP dust model,} \\ \tau &= 0.062 \pm 0.012 \text{ Ka, Q and V cleaned by 353 GHz,} \\ \tau &= 0.063 \pm 0.020 \text{ LFI 70 GHz,} \\ \tau &= 0.051 \pm 0.009 \text{ HFI } 100 \times 143 \text{ GHz,} \end{aligned} \quad (1)$$

the first value reported represents the final bound of WMAP Collaboration; the second is the most recent WMAP bound when the *Planck* 353 GHz map is used for the thermal dust cleaning; the last two values represent the *Planck* 2018 legacy release bounds obtained using respectively LFI and HFI.

In this paper, we present an advanced approach to the *Planck* HFI data in the attempt of reducing the systematic effects affecting the large scale polarization with the purpose of improving and solidifying the constraints of  $\tau$ . We upgrade the SRo11 map-making algorithm introduced in *Planck Collaboration Int. XLVI* (2016) (hereafter SRo11) with a new cleaning of residual distortions of the large signals, we call this new algorithm SRo12 (*Delouis et al.* 2019).

The paper is organized as follow: in Section 2, we present the improved mapmaking algorithm. In Sections 3 and 4, we present the power spectra, the main result on  $\tau$ , and the consistency tests performed. Finally, in Section 5, we show the impact of the new  $\tau$  constrain on the cosmological scenario.

## 2. Map-making improvements

The 2018 legacy HFI maps (*Planck Collaboration III* 2019) represent a great step forward in the attempt of cleaning systematic effects contaminating the large scale polarization. In particular, the impact of the non-linearities of the analogue-to-digital converters (ADCs) of readout chains has been substantially reduced, introducing variation in the gain of bolometer readout chains. This correction accounts for the first-order approximation of the ADC non-linearity (ADCNL) systematic effect, but still, large signals, such as foregrounds on the Galactic plane and dipoles, are affected by the second-order ADCNL effect. This was not treated by the *Planck* Collaboration (see Section 5.13 of *Planck Collaboration III* (2019) for details), leaving large scale residuals in polarization mainly due to a mismatch that, violating

the stationarity of the signal in a given pixel, causes temperature to polarization dipole leakage.

For the analysis presented in this paper, we improve the SRo11 code in what we call SRo12, in order to further reduce the polarization leakage due to strong signals. In the following, we list the main modifications introduced in the SRo12 code, for more details, see *Delouis et al.* (2019):

- New ADCNL correction is obtained by fitting the residuals with a bi-dimensional spline model per bolometer as a function of signal value and time. This solution removes the apparent gain variation of bolometers allowing to fit only one gain for the entire mission. As demonstrated in *Delouis et al.* (2019), time variation is only necessary to capture the ADCNL at 143 GHz, and thus for the 100 and 353 GHz bolometers, only a mono-dimensional spline is considered. We verify that, for those channels, opening the time variation does not improve substantially the solution.
- Internal fit of (and subsequently marginalization over) the polarization angle and polarization efficiency per bolometer.
- Update of the CO template based on 2015 *Planck* release, used for the bandpass mismatch fit, introducing two new templates based on <sup>12</sup>CO and <sup>13</sup>CO extracted as described in *Planck Collaboration III* (2019) section 3.1.3 and in *Delouis et al.* (2019) section 4.1.
- Update of the thermal dust template using a map based on 2018 legacy release (for details, see section 4.1 of *Delouis et al.* (2019)).
- Update of the real part of the empirical transfer function used at 353 GHz, replacing the 3 real harmonic ranges of the spin frequency used in the *Planck* 2018 legacy release (see *Planck Collaboration III* (2019) section 2.2.2) by a single 10s time constant (for details see section 4.2.2 of *Delouis et al.* (2019)).

Figure 1 shows polarization intensity maps (defined as  $P \equiv \sqrt{Q^2 + U^2}$ ) at 100 and 143 GHz obtained simulating realistic sky signal affected by ADCNL and projected with SRo11 and SRo12 codes. From those maps, we remove the input sky. In the first row, we show maps obtained with SRo11 without gain variation. In the middle row, the maps are obtained using SRo11 opening the gain variation and fitting 128 gain steps as done in *Planck Collaboration III* (2019). In the last row, the simulated timelines are projected into maps with the SRo12 code. The large scale dipole leakage present in the first panel is substantially reduced by the introduction of gain variability (second panel) which still leaves  $\sim 1\mu\text{K}$  level residuals as already shown *Planck Collaboration III* (2019). This residual is further reduced by SRo12 demonstrating that the ADC-NL correction allows to fit a single gain for the bolometers as expected from pre-flight analysis (*Holmes et al.* 2008; *Pajot et al.* 2010; *Catalano et al.* 2010).

In Figure 2, we report the  $EE$  pseudo power spectra ( $\mathcal{D}_\ell \equiv \ell(\ell + 1)C_\ell/2\pi$ ) of the residual systematic effects (hereafter systematics) maps shown in Fig. 1. The level of those residuals is pushed below  $2 \times 10^{-2} \mu\text{K}^2$  both for 100 and 143 GHz by SRo12, gaining an order of magnitude with respect to SRo11 results. Furthermore, those residuals are weakly correlated, as can be seen in Fig. 3. In the  $100 \times 143$   $EE$  cross-spectrum, the level of systematics is further reduced below  $3 \times 10^{-3} \mu\text{K}^2$  (green line of Fig. 3). With SRo12, systematics are negligible with respect

<sup>1</sup>A more conservative analysis based on pseudo- $C_\ell$  estimator (*Hivon et al.* 2002; *Tristram et al.* 2005) is presented in *Planck Collaboration Int. XLVII* (2016) which reports  $\tau = 0.058 \pm 0.012$ .

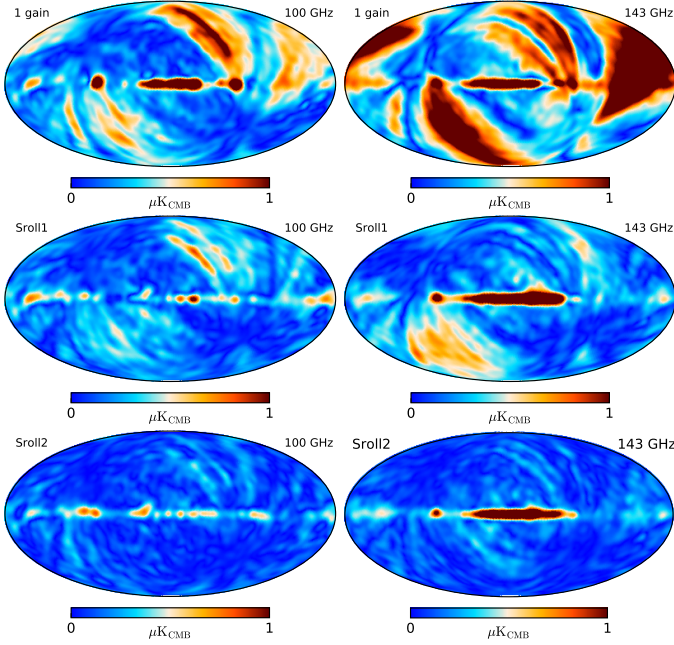


**Fig. 1.** Polarization intensity maps at 100 and 143 GHz obtained applying SRoll1 and SRoll2 to a set of simulated timelines. The input sky has been subtracted after the map projection. The simulated timelines contain dipole, sky signal, systematic effects and electronic noise only. The first row shows maps obtained running SRoll1 with only one gain for the entire mission, the middle row shows SRoll1 with 128 gain steps, as used in *Planck* 2018 legacy release, and last one shows SRoll2 results.

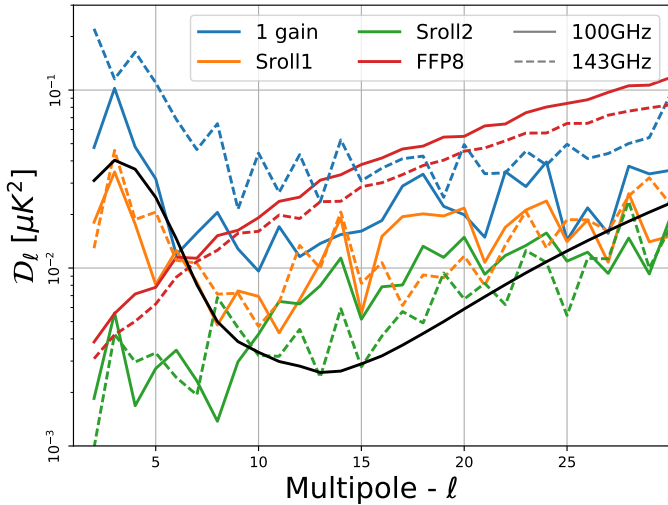


**Fig. 2.**  $EE$  pseudo auto-spectra evaluated for 100 GHz (solid) and 143 GHz (dashed) on the simulations shown in Fig. 1. Here we have applied a symmetric Galactic cut of  $20^\circ$ , retaining 66% of the sky. The rise at higher multipoles is caused by the autocorrelation of the electronic noise present in the maps which is not debiased. The red lines represent the average of 100 FFP8 simulations (Planck Collaboration XII 2016) containing only white noise and  $1/f$  noise. The black solid line corresponds to a  $EE$  power spectrum with  $\tau = 0.055$ .

to a typical CMB power spectrum and below the gaussian noise level<sup>2</sup>.

<sup>2</sup>The noise spectrum shown in Fig. 3 should not be interpreted as noise level biasing the cross-spectrum estimate, by definition unbiased,

Besides, we start to be limited by the quality of the dust template, given that the level of residual systematic effects in the  $100 \times 143$  spectrum (green line of Fig. 3) is below or at most equal to the systematics still present in the 353 GHz channel used as dust template for both 100 and 143 GHz (purple line).

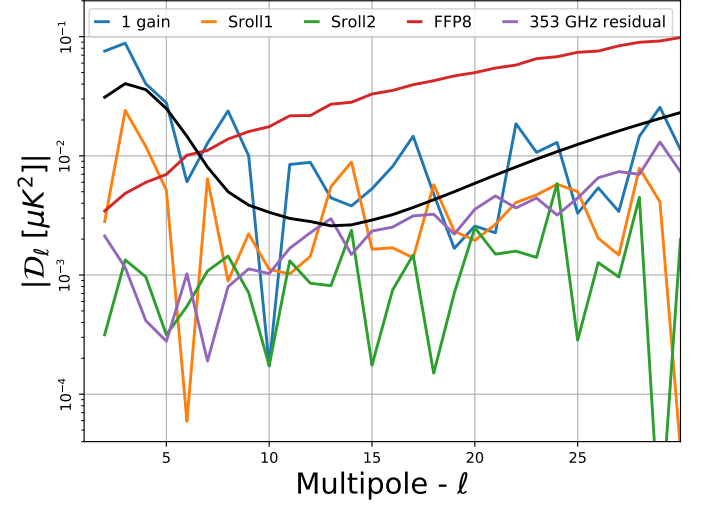


**Fig. 3.** As Fig. 2 but for the pseudo  $100 \times 143$  cross-spectra. In purple, we plot the auto-spectrum of 353 GHz residual systematic effects rescaled to  $100 \times 143$  ( $\sim 8 \times 10^{-4}$  factor applied,  $\sim 0.02$  from 100 GHz and  $\sim 0.04$  from 143 GHz). The red line is the square root of the product of 100 and 143 GHz noise spectra that is proportional to the variance associated with the noise in the cross-spectrum. In the SRoll2 maps, the large scale is dominated by signal and  $1/f$  noise rather than residual systematic effects.

Similar improvement is easily recognizable in SRoll2 maps of data. In Figures 4 and 5, we show 100 and 143 GHz maps after the removal of diffuse Galactic foreground contamination for both SRoll1 and SRoll2. The overall level of systematics is significantly reduced everywhere in the maps by SRoll2. Both the large scale spurious structures associated to dipole leakage and the Galactic disc residuals are substantially improved.

### 3. Power spectrum

This section describes the power spectrum computation made using SRoll2 maps and the analysis performed on simulations. As a general approach, we follow the procedure adopted for HFI low- $\ell$  analysis presented in Planck Collaboration V (2019) (section 2.2). In short, 100 and 143 GHz maps, built only using polarization sensitive bolometers (PSBs), undergo the following procedure:

- We filter them with a cosine window function (Benabed et al. 2009; Planck Collaboration Int. XLVI 2016), downgrading to HEALPix (Górski et al. 2005)  $N_{\text{side}} = 16$  resolution. In order to maintain the covariances invertible, we add  $20 \text{ nK}$  of diagonal regularization noise.
- We remove the Galactic foreground contamination through template fitting. We employ SRoll2 353 GHz map for thermal dust removal and, WMAP 9yr K and Ka bands for

but as noise contribution entering, together with the theoretical CMB spectrum, in the error computation.

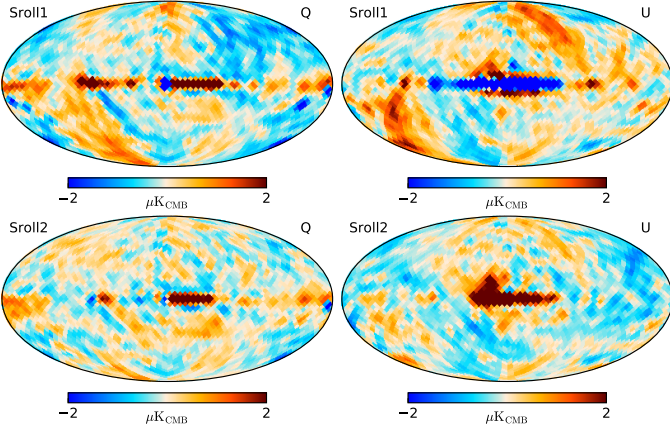


**Fig. 4.** Data Q and U maps at 100 GHz cleaned from synchrotron and dust emissions. Top row shows the *Planck* 2018 legacy release computation obtained with SRoll1, while the bottom one the SRoll2 computation.

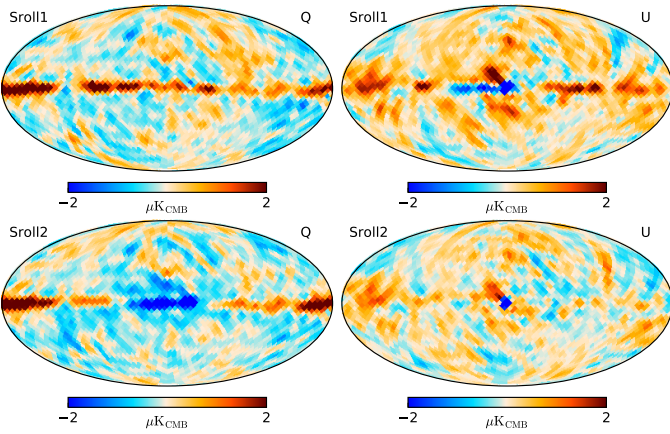


**Fig. 5.** Data Q and U maps at 143 GHz cleaned from synchrotron and dust emissions. Top panel shows the *Planck* 2018 legacy release computation obtained with SRoll1, while the bottom one the SRoll2 computation.

synchrotron at 100 and 143 GHz respectively. The scalings found are reported in Tab. 1

- We compute the cross-QML (Planck Collaboration V 2019; Tegmark 1996; Tegmark & de Oliveira-Costa 2001; Efstathiou 2006) power spectrum between 100 and 143 GHz cleaned maps (see Fig. 7) outside a Galactic mask (see Fig. 6). As temperature map, we use the *Planck* 2018 Commander solution (Planck Collaboration IV 2019; Planck Collaboration V 2019) smoothed with a  $440'$  ( $\sim 7.3^\circ$ ) gaussian beam and regularized with  $2\mu\text{K}$  diagonal noise. As covariance matrices, we use FFP8 covariances (Planck Collaboration VIII 2016; Planck Collaboration XII 2016) for the HFI channels, and for WMAP K and Ka, the official 9yr matrices (Bennett et al. 2013).

The same cleaning procedure is applied to a set of 500 Monte Carlo simulations containing realistic sky signal, noise and systematic effects. The fiducial CMB map contained in those simulations is removed after the foreground cleaning leaving only maps with noise, systematic effects and foreground residuals, referred hereafter as N+S+F-MC (for Noise, Systematics and Foreground residuals Montecarlo).

**Table 1.** Template scalings measured on data. The synchrotron tracers are WMAP K and Ka bands for 100 and 143 GHz respectively. The dust tracer is the 353 GHz map.

Channel [GHz]	$\alpha \times 10^2$	$\beta \times 10^2$
100 . . . . .	$0.95 \pm 0.07$	$1.86 \pm 0.015$
143 . . . . .	$1.63 \pm 0.21$	$0.0394 \pm 0.014$

As already stated in Planck Collaboration Int. XLVI (2016) and Planck Collaboration V (2019), FFP8 covariance matrices (Planck Collaboration XII 2016) represent a sub-optimal, but unavoidable, choice. The FFP8 covariance matrices are built following the method presented in Keskitalo et al. (2010) (see in particular section 3.2). They are assembled in two pieces, one describing the sub-baseline correlation part which is untouched by the destriper mapmaking and one describing the ring-to-ring correlation due to errors in solving for the baselines. Consequently those matrices do not capture properly the variance of the systematic effects but only the white and  $1/f$  noise components, assuming an analytical model for the noise spectrum<sup>3</sup>. Despite that, since we rely on cross-spectrum estimator, this choice does not impact power spectrum estimate but only its optimality (see e.g. Planck Collaboration Int. XLVI (2016); Planck Collaboration V (2019)).

Furthermore, for SRoll2 maps, having the residual systematics further reduced with respect to noise (see Fig. 3), we have a more efficient estimator than the analysis performed for *Planck* 2018 legacy release.

All masks used for foreground cleaning (see Fig. 6), power spectrum estimation and likelihood are obtained thresholding the sum of dust polarization intensity scaled at 143 GHz with synchrotron polarization intensity scaled at 100 GHz, both smoothed with a Gaussian window function with full width maximum of  $7.5^\circ$ . As dust and synchrotron tracers, we use *Planck* 353 GHz, scaled by  $\beta = 0.039$  and WMAP K band, scaled by  $\alpha = 0.0095$ . The mask used for the foreground template fitting, both for data and simulations, retains 70% of the sky. The other masks are used in the cosmological analysis.

Figure 7 shows the  $100 \times 143$   $EE$  power spectrum of the SRoll2 maps compared with the *Planck* 2018 power spectrum both on 50% of the sky. The error bars are obtained combining a Monte Carlo of CMB signal with  $\tau = 0.055$  with N+S+F-MC, and computing the QML power spectrum from all the maps. The quadrupole affecting *Planck* 2018 analysis is radically reduced by the new map-making procedure.

In Fig. 8, we compare the error bars purged from cosmic variance obtained in SRoll2 maps with the ones of *Planck* 2018 analysis. With the SRoll2 maps, we manage to halve quadrupole and octupole errors with respect to the *Planck* 2018 analysis. Overall the entire range of multipoles sensitive to reionization optical depth shows a clearly reduced level of residual systematic effects and a lower variance. Furthermore, the  $C_{\ell S}$  are weakly correlated as shown in Fig. 9. In the range relevant for  $\tau$  estimation  $\ell = [2 \dots 8]$ , the multipoles are substantially uncorrelated, with the scatter observed in the off-diagonal correlation perfectly compatible with the number of N+S+F-MC simulations. In the region where the  $EE$  signal is expected to be very small in  $\Lambda\text{CDM}$  model ( $\ell = [10 \dots 20]$ ) we notice the presence of a weak (up to 20%)  $\ell, \ell + 2$  correlation, nevertheless this feature is not expected to affect substantially the  $\tau$  estimation.

<sup>3</sup>FFP8 covariance matrices can be obtained upon specific request to the *Planck* Project Scientist at ESTEC or directly to NERSC.

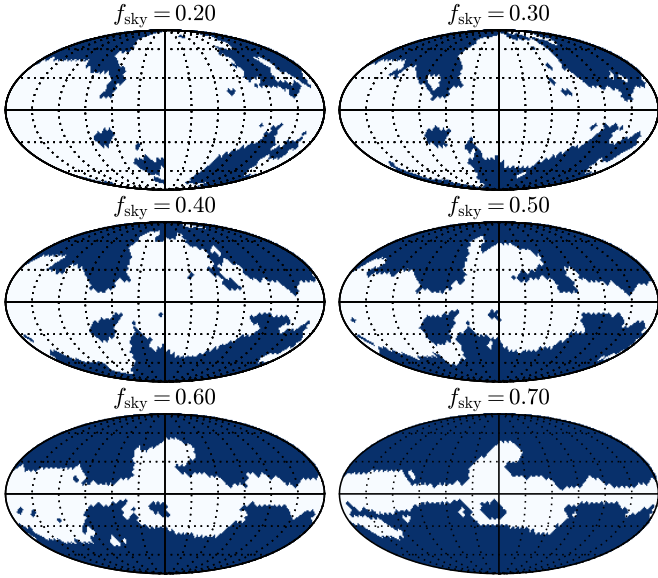


**Fig. 6.** Masks used for the present analysis. The 70% mask is used for the foreground cleaning, the others in the cosmological analysis. All the masks used in this analysis are binary maps, without any apodization applied.

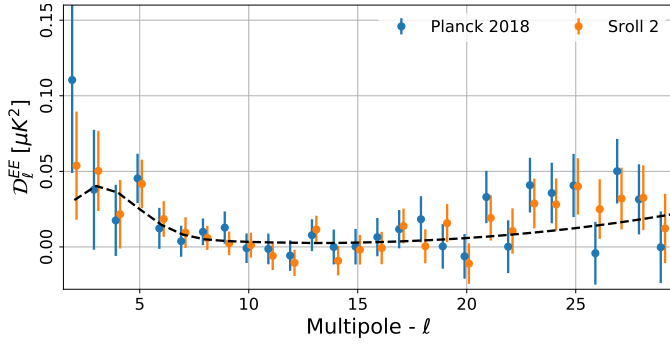


**Fig. 7.** Low- $\ell$   $EE$  cross spectrum  $100 \times 143$  for the *Planck* 2018 legacy release (blue points) and for the SRoll2 maps (orange). The mask used retains 50% of the sky. The error bars are Monte Carlo based and do include cosmic variance. The black line corresponds to a  $EE$  power spectrum with  $\tau = 0.055$ .

By comparing the fraction of the error due to noise and systematic effects with the cosmic variance for  $\tau = 0.055$ , in the range  $\ell = [2 \dots 6]$ , we notice that, for the first time, we start being dominated by the latter, as shown in Fig. 10. All the error bars are obtained using simulations and not computed analytically.

In Fig. 11, we compare  $EE$  power spectrum obtained with different masks. The multipole  $\ell = 5$  shows the largest variation throughout the various masks. We verify, using simulations, that this variation is always consistent with  $2\sigma$  fluctuation. We emphasize again that N+S+F-MC contains noise, systematic effects and residuals of foreground cleaning.

As final test, we show in Fig. 12 the  $BB$  power spectrum obtained from the cross-correlation of 100 and 143 GHz SRoll2 maps. As reference, we jointly plot *Planck* 2018 legacy release  $BB$  power spectrum (*Planck Collaboration V 2019*). Both spectra are compatible with null signal, with SRoll2 being more constraining at very large scale. The probability to exceed is PTE=0.73, for *Planck* 2018, and PTE=0.86, for SRoll2. The large negative quadrupole in *Planck* 2018 legacy release, related to ADCNL residuals (see *Planck Collaboration III (2019)*

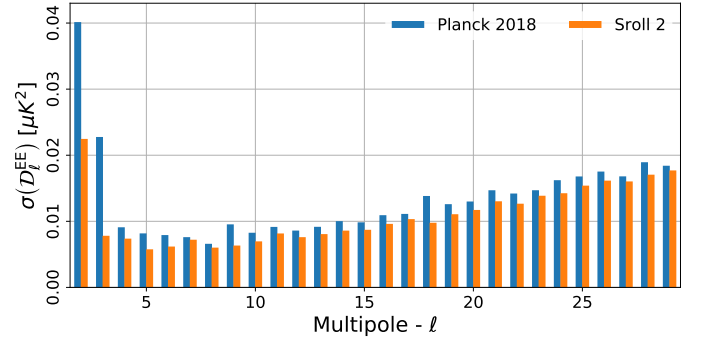


**Fig. 8.** Comparison between *Planck* 2018 legacy release and SRoll2 error bars for  $100 \times 143$  spectrum both on 50% of the sky. For SRoll11 *Planck* 2018 FFP10 *Planck Collaboration III (2019)* simulations have been used, for SRoll12 N+S+F-MC simulations presented in *Delouis et al. (2019)*. Cosmic variance here is not included.

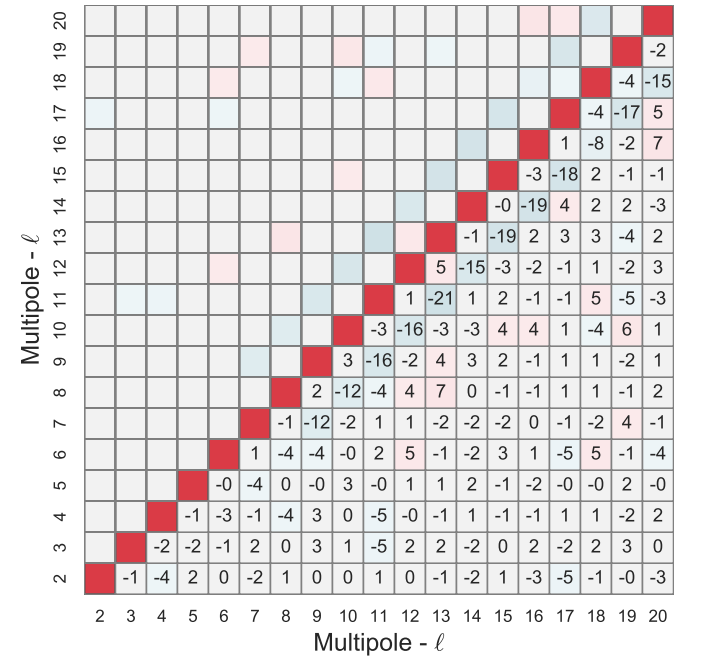


**Fig. 9.** Correlation matrix in [%] for  $EE$  power spectrum below  $\ell = 20$  estimated from 500 signal (with  $\tau = 0.055$ ) + N+S+F-MC simulations. The different multipoles are substantially uncorrelated.

and *Planck Collaboration V (2019)*), is almost completely reabsorbed in the new analysis. As final test, assuming the empirical distribution of the N+S+F-MC simulations and the power spectra measured on data computed on the 50% mask, in Tab. 2 we report,  $\ell$ -by- $\ell$ , the percentage of simulations that have an absolute value of the difference between  $\mathcal{D}_\ell$  and the barycenter of the distribution larger than the same quantity measured on data. Also in this case, the overall agreement is excellent, with no particular outliers.

#### 4. Likelihood and $\tau$ estimation

Following the procedure presented in *Planck Collaboration V (2019)*, we build a likelihood for  $\tau$ , based on  $100 \times 143$   $EE$  power spectrum in the multipole range  $2 - 29$ . In details:

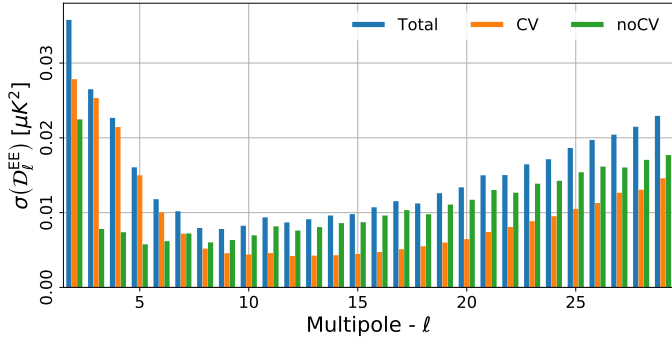


**Fig. 10.** Error comparison for the  $100 \times 143$  spectrum on 60% of the sky. We show the total error (blue bar), the amount solely due to cosmic variance (orange), and only due to noise and systematic effects (green). The cosmic variance shown corresponds to  $\tau = 0.055$ .

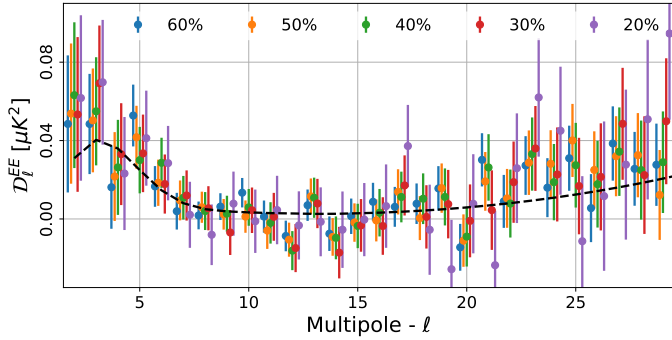


**Fig. 11.**  $EE$  power spectra of  $100 \times 143$  for different sky fractions. Error bars are obtained from the distribution of 500 signal (with  $\tau = 0.055$ ) + N+S+F-MC simulations. The black solid line corresponds to a  $EE$  power spectrum with  $\tau = 0.055$ .

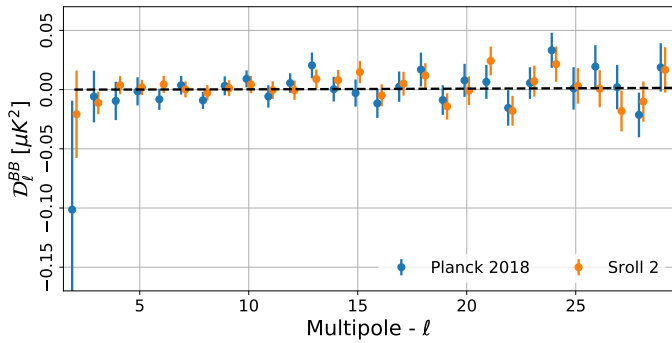


**Fig. 12.** Low- $\ell$   $BB$  cross spectrum  $100 \times 143$  for the *Planck* 2018 legacy release (blue points) and for the Sroll12 maps (orange). The mask used retains 50% of the sky. The error bars are Monte Carlo based and do include cosmic variance.

- we generate 101 theoretical power spectra,  $C_\ell^{\text{th}}(\tau, \theta)$ , equally spaced in the range  $\tau = [0, 0.1]$ , varying accordingly  $A_s$  such that  $10^9 A_s e^{-2\tau} = 1.875$  as in [Planck Collaboration Int. XLVI \(2016\)](#). The other  $\Lambda$ CDM cosmological parameters ( $\theta$ ) are fixed to the best fit model of [Planck Collaboration VI \(2019\)](#);
- for each  $C_\ell^{\text{th}}(\tau, \theta)$ , we build a CMB signal Monte Carlo of 500 maps;
- we combine N+S+F-MC with the signal Monte Carlo, and we compute the  $100 \times 143$   $EE$  spectrum for each realization. We compute the power spectrum also for data,  $C_\ell^{\text{data}}$ ;

**Table 2.** Percentage of signal plus N+S+F-MC simulations that  $\ell$ -by- $\ell$  have absolute difference between  $\mathcal{D}_\ell$  and the mean of the empirical distribution larger than the data.

Multipole	TE	EE	BB	TB	EB
2	58.1	38.0	76.5	87.5	56.2
3	72.2	20.4	6.8	42.8	90.9
4	52.8	62.5	50.1	88.5	53.9
5	28.7	93.4	52.7	23.6	27.7
6	77.7	67.1	85.4	48.2	99.8
7	93.1	91.4	35.9	68.8	72.7
8	94.2	55.4	56.0	22.7	35.5
9	99.4	83.2	12.8	43.8	93.2
10	75.0	59.1	99.3	52.1	5.6
11	16.3	62.6	46.9	37.0	52.5
12	13.9	76.8	74.1	67.2	23.7
13	24.5	32.0	95.7	91.1	39.9
14	16.9	32.4	83.5	1.8	61.8
15	52.1	12.8	98.6	2.9	7.3
16	71.5	45.4	87.0	78.9	65.7
17	38.4	75.6	89.4	86.8	59.3
18	61.4	42.3	4.1	5.9	2.4
19	32.3	13.7	11.9	84.5	14.4
20	25.6	81.2	97.5	52.3	24.0
21	43.4	8.0	70.6	31.6	51.0
22	92.5	13.4	24.7	84.6	64.0
23	34.5	68.8	91.5	22.4	35.6
24	28.8	22.3	6.1	51.9	33.6
25	17.5	93.8	40.9	15.8	57.6
26	55.4	89.1	15.1	88.1	14.5
27	55.5	21.0	84.7	3.2	26.1
28	54.6	44.4	6.4	36.2	25.2
29	76.9	57.4	86.5	88.3	91.8

- histogramming the simulations  $\ell$ -by- $\ell$  and  $\tau$ -by- $\tau$ , we build empirically the probability  $\mathcal{P}(C_\ell|\tau; \theta)$ ;
- with a piecewise polynomial function  $f_\ell(C_\ell; \tau, \theta)$  we interpolate  $\ln \mathcal{P}(C_\ell|\tau; \theta)$  in order to smooth the scatter due to limited number of simulations available;
- assuming negligible correlation between multipoles (see [Fig. 9](#)), we compute the probability for each  $\tau$  value in our grid:

$$\mathcal{P}(\text{data}|\tau; \theta) = \exp\left(\sum_{\ell=2}^{29} f_\ell(C_\ell^{\text{data}}; \tau, \theta)\right). \quad (2)$$

With this algorithm, we can draw slices of probability for  $\tau$  adopting different sky fractions and multipole ranges, in order to stress the stability of the analysis and to perform consistency tests.

As a first consistency check, we test how the sky fraction used to compute the power spectrum impacts the  $\tau$  constraint. We explore the same masks used in [Fig. 11](#) and shown in [Fig. 6](#). In [Fig. 13](#), we show a whisker plot with best-fit values, 68% and 95% confidence levels on  $\tau$  for spectra computed with different QML masks, ranging from 20 to 60% of used sky. The  $\tau$  posteriors are stable, all within one  $\sigma$ . We verify on simulations the statistical consistency of the  $\tau$  values computed on different masks, finding a consistency always better than  $1.3 \sigma$  throughout the various masks, having accounted for the common sky, noise and systematics. As baseline, we adopt the 50% mask where we measure a reionization optical depth of:

$$\tau = 0.0566_{-0.0062}^{+0.0053} \quad (68\%, \text{ Sroll2 } EE \text{ spectrum}), \quad (3)$$

having fixed  $10^9 A_s e^{-2\tau} = 1.875$ .

In the following part of this section, we show tests performed only on the 50% sky mask.

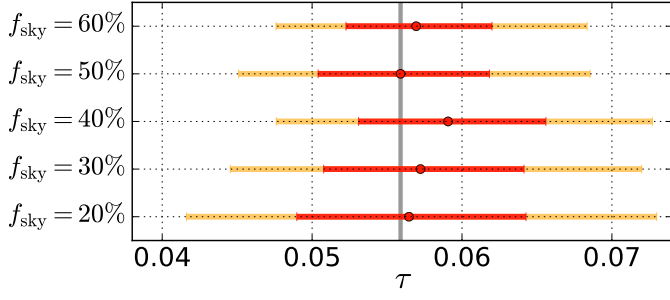


**Fig. 13.** Values of  $\tau$  obtained varying the sky fraction used for power spectrum estimation of  $100 \times 143$ . In this and the following plots the round points represent best-fit values and, red and yellow bars 68% and 95% C.L. respectively.

Figure 14 shows the effect of changing the minimum multipole used in Eq. 2. The  $\tau$  posteriors are stable up to  $\ell_{\min} = 5$ , further explorations being less meaningful due to the drop of the reionization feature above those multipoles.

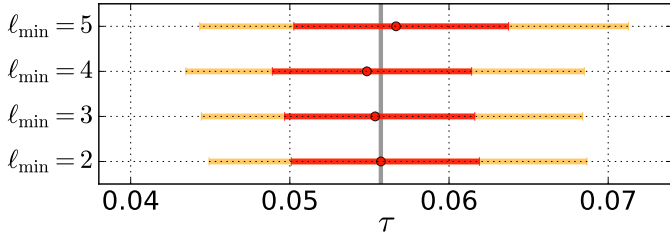


**Fig. 14.** Values of  $\tau$  obtained changing the minimum multipole used in the likelihood code.

In Fig. 15, we test the stability of  $\tau$  posterior when one multipole at a time is removed from the summation in Eq. 2. The maximum variation is observed when  $\ell = 5$  is removed causing a roughly half- $\sigma$  shift in the  $\tau$  posterior. This shift was consistently observed by analogous analysis performed on previous versions of the same HFI data (see e.g. [Planck Collaboration Int. XLVI \(2016\)](#) figure D.9 and [Planck Collaboration V \(2019\)](#) figure 14) with SR0112 being less discrepant despite the smaller overall error budget. Also in this case, we verify on simulations that the  $\tau$  obtained removing  $\ell = 5$  is consistent with a  $1.2\sigma$  statistical fluctuation when compared with the one obtained using the full range.

We also explore the stability of the  $\tau$  constraint changing the synchrotron tracers used respectively for 100 and 143 GHz. In figure 16 we show  $\tau$  posteriors obtained using different combinations of the available synchrotron tracers, WMAP K band, WMAP Ka band or LFI 30 GHz ([Planck Collaboration II 2019](#)), all the posteriors are extremely consistent demonstrating that the synchrotron subtraction does not represent a critical point, as already discussed in [Planck Collaboration V \(2019\)](#).

We tested the quality of the dust removal employing the 217 GHz instead of 353 GHz for the cleaning of 100 GHz. In figure 17 we compare the  $\tau$  posterior obtained cleaning both 100 and 143 GHz using 353 GHz with the one obtained by cleaning 100 GHz with 217 GHz and 143 GHz with 353 GHz. The consistency is remarkable, with only the latter showing slightly larger

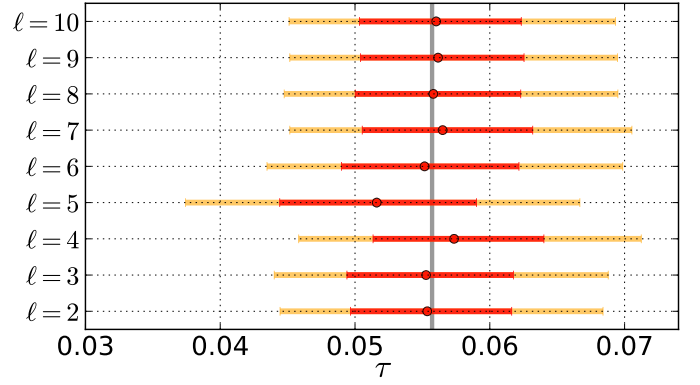


**Fig. 15.** Posteriors of  $\tau$  obtained removing one multipole at a time.

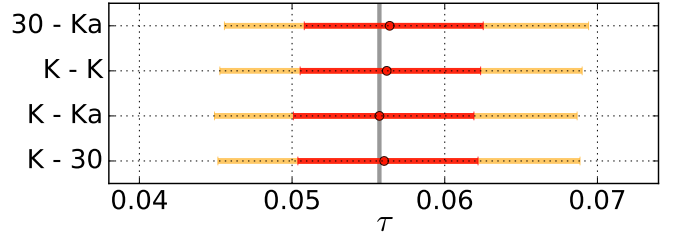


**Fig. 16.** Posteriors of  $\tau$  obtained using different synchrotron tracers for 100 and 143 GHz. The channels reported on the left side of the figure refer to the synchrotron tracers used for 100 and 143 GHz respectively.

error bars, likely due to the smaller leverage of 217 GHz not fully compensated by the lower noise.

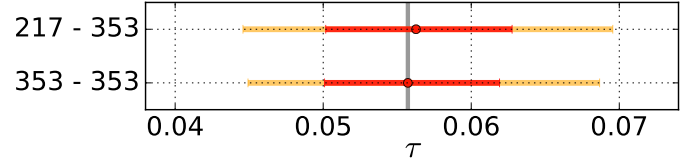


**Fig. 17.** Posteriors of  $\tau$  obtained using different dust tracers for 100 GHz. Similarly to what show in Fig. 16 the channels reported in the y-axis label refer to the dust tracers used respectively for 100 and 143 GHz.

Finally, we attempt a similar analysis on the  $TE$  spectrum only, measuring  $\tau$  for the same 50% mask, finding:

$$\tau = 0.057^{+0.012}_{-0.013} \quad (68\%, \text{ SR0112 } TE \text{ spectrum}), \quad (4)$$

which nicely confirms the  $EE$  based result. It is worth to mention here that the poor PTEs for the null TE spectra found in the *Planck* 2018 likelihood analysis ([Planck Collaboration V 2019](#)) are still present in this version of the data, even if with slightly less significance. We recall also that we employ the same Commander solution used in the *Planck* 2018 likelihood, thus based on SR0111 maps.

## 5. Impact on cosmology

Following the method presented in [Planck Collaboration V \(2019\)](#) and used for the *Planck* SimAll likelihood (i.e. lowE in

*Planck* 2018 legacy release) we build a likelihood for SRoll2 100x143 EE power spectrum<sup>4</sup>. We call this new likelihood module lowE-S2<sup>5</sup>.

Superseding the *Planck* lowE likelihood, we combine the lowE-S2 with the high- $\ell$  Plik 2018 likelihood and with the Commander 2018 low- $\ell$  temperature likelihood in order to constrain cosmological parameters. In this section, we explore the cosmological parameter space making use of the cosmomc<sup>6</sup> package (Lewis & Bridle 2002) based on camb<sup>7</sup> Boltzmann code (Lewis et al. 2000). The global settings in terms of parametrization and assumptions are coherent with *Planck* Collaboration VI (2019).

First of all, we combine lowE-S2 with only with Commander 2018 temperature likelihood, and we estimate the cosmological parameters only sampling  $\ln(10^{10}A_s)$  and  $\tau$ , keeping fixed the other parameters to *Planck* TT+lowE bestfits, measuring

$$\tau = 0.0579_{-0.0067}^{+0.0056} \quad (68\%, \text{ Commander TT+lowE-S2}), \quad (5)$$

which is directly comparable with the bounds shown in Eq. 1. The amplitude of the scalar perturbations preferred by the temperature likelihood is substantially low (see e.g. *Planck* Collaboration V (2019) Table 4 and 12) which is compensated by an increase of the  $\tau$  value. Opening the other  $\Lambda$ CDM parameters, and adding the TT likelihood drives the value of  $\tau$  upwards

$$\tau = 0.0575_{-0.0069}^{+0.0056} \quad (68\%, \text{ TT+lowE-S2}), \quad (6)$$

Similar behaviour was also observed in *Planck* Collaboration VI (2019) and *Planck* Collaboration XIII (2016) and is mainly due to the  $A_s e^{-2\tau}$  degeneracy broken by the high- $\ell$  lensing in the temperature spectrum. The addition of high- $\ell$  polarization drives again upward  $A_s$  and thus the optical depth up to:

$$\tau = 0.0591_{-0.0068}^{+0.0054} \quad (68\%, \text{ TT,TE,EE+lowE-S2}). \quad (7)$$

The fluctuation amplitude can be directly constrained at late times by CMB lensing reconstruction power spectrum (*Planck* Collaboration VIII 2019), partially degenerated with the matter density, while the BAO measurements constrain very efficiently the geometry of the late universe (see *Planck* Collaboration VI (2019) for more details on those datasets). Nonetheless the combination of *Planck* 2018 lensing likelihood and BAO measurements with the primary CMB anisotropies does not improve significantly the  $\tau$  constraint:

$$\tau = 0.0599_{-0.0064}^{+0.0054} \quad (68\%, \text{ TT,TE,EE+lowE-S2+Lensing+BAO}). \quad (8)$$

Assuming a tanh parametrization of the ionization fraction, the  $\tau$  constrain can be translated into a mid-point redshift of reionization of:

<sup>4</sup>For details about validation and performances of the likelihood approximation see Gerbino et al. (2019).

<sup>5</sup>The likelihood module is built within the clik infrastructure (*Planck* Collaboration XV 2014; *Planck* Collaboration ES 2013, 2015, 2018) and it is available on <http://sroll20.ias.u-psud.fr> or on [https://web.fe.infn.it/~pagano/low\\_ell\\_datasets/sroll2](https://web.fe.infn.it/~pagano/low_ell_datasets/sroll2)

<sup>6</sup><http://cosmologist.info/cosmomc>

<sup>7</sup><http://camb.info>

$$z_{\text{re}} = 8.21 \pm 0.58 \quad (68\%, \text{ TT,TE,EE+lowE-S2+Lensing+BAO}), \quad (9)$$

consistent with the latest astrophysical constraint of high-redshift quasars (see e.g. Becker et al. (2001), Fan et al. (2006) and Bouwens et al. (2015) for an exhaustive comparison).

The combination of low and high- $\ell$  likelihoods breaks efficiently the  $A_s e^{-2\tau}$  degeneracy, giving:

$$\ln(10^{10}A_s) = 3.054 \pm 0.012 \quad (68\%, \text{ TT,TE,EE+lowE-S2+Lensing+BAO}). \quad (10)$$

In the context of  $\Lambda$ CDM model, this bound can be directly translated in the  $\sigma_8$  parameter

$$\sigma_8 = 0.8128 \pm 0.0053 \quad (68\%, \text{ TT,TE,EE+lowE-S2+Lensing+BAO}), \quad (11)$$

which measures the amplitude of the matter power spectrum on the scale of  $8h^{-1}\text{Mpc}$ .

Bounds on the  $\Lambda$ CDM native parameters and some meaningful derived ones are reported in Tab. 3 where we compare the results obtained with the *Planck* 2018 baseline likelihood with the ones obtained replacing lowE with lowE-S2.

We also consider minimal one parameter extensions of the  $\Lambda$ CDM model such as  $\Omega_K$ ,  $\Sigma m_\nu$ ,  $N_{\text{eff}}$  and  $Y_{\text{He}}$  finding no relevant changes with respect to the *Planck* 2018 legacy release bounds (*Planck* Collaboration VI 2019) which reinforce the overall stability of the *Planck* 2018 results. This is likely to be connected to the mostly unchanged upper limit on  $\tau$ , i.e.  $\tau \lesssim 0.07$  at 95% C. L..

Finally, we explore the phenomenological parameter  $A_L$  which rescales the lensing potential with respect to the theoretical expectation within  $\Lambda$ CDM model. Consistently throughout *Planck* releases the CMB power spectra show a preference for  $A_L > 1$  (*Planck* Collaboration XVI 2014; *Planck* Collaboration XIII 2016; *Planck* Collaboration VI 2019), see *Planck* Collaboration Int. LI (2017) for extensive discussion. Such values of  $A_L$  are in slight tension with the theoretical expectations and with the ones extracted from the lensing reconstruction power spectrum (*Planck* Collaboration VIII 2019). Combining temperature and polarization data, in the *Planck* 2018 legacy release,  $A_L = 1.180 \pm 0.065$  was measured. Replacing lowE with lowE-S2 slightly reduces the lensing amplitude down to  $A_L = 1.163 \pm 0.064$ , without changing the overall conclusions of *Planck* Collaboration VI (2019). This is again explainable with the increase of  $A_s$  connected with the increase of  $\tau$  which allows a slightly lower lensing amplitude.

## 6. Conclusions

In this paper we present an improved constraint on the reionization optical depth  $\tau$ , obtained analyzing the *Planck* HFI data with an updated version of the SRoll1 map-making algorithm called SRoll2 specifically designed to reduce the residual large scale polarization systematics still present in the *Planck* HFI 2018 legacy maps. Details and performances of the SRoll2 algorithm are described extensively in Delouis et al. (2019).

The level of residual systematics associated to the first multipoles, relevant for  $\tau$  estimation, is brought below the noise level and for the first time the cosmic variance becomes the main

**Table 3.** Parameter constraints for the base  $\Lambda$ CDM cosmology (as defined in [Planck Collaboration XVI 2014](#)), illustrating the impact of replacing the lowE likelihood with the lowE-S2 likelihood presented in the paper. We also show the change when including the high- $\ell$  polarization.

Parameter	TT+lowE 68 % limits	TT+lowE-S2 68 % limits	TTTEEE+lowE 68 % limits	TTTEEE+lowE-S2 68 % limits
$\Omega_b h^2$ . . . . .	$0.02212 \pm 0.00022$	$0.02214 \pm 0.00021$	$0.02236 \pm 0.00015$	$0.02237 \pm 0.00015$
$\Omega_c h^2$ . . . . .	$0.1206 \pm 0.0021$	$0.1205 \pm 0.0021$	$0.1202 \pm 0.0014$	$0.1201 \pm 0.0013$
$100\theta_{MC}$ . . . . .	$1.04077 \pm 0.00047$	$1.04080 \pm 0.00047$	$1.04090 \pm 0.00031$	$1.04090 \pm 0.00031$
$\tau$ . . . . .	$0.0522 \pm 0.0080$	$0.0574^{+0.0056}_{-0.0069}$	$0.0544^{+0.0070}_{-0.0081}$	$0.0591^{+0.0054}_{-0.0068}$
$\ln(10^{10} A_s)$ . . . . .	$3.040 \pm 0.016$	$3.051 \pm 0.013$	$3.045 \pm 0.016$	$3.054 \pm 0.013$
$n_s$ . . . . .	$0.9626 \pm 0.0057$	$0.9631 \pm 0.0056$	$0.9649 \pm 0.0044$	$0.9651 \pm 0.0043$
$H_0$ . . . . .	$66.88 \pm 0.92$	$66.95 \pm 0.90$	$67.27 \pm 0.60$	$67.32 \pm 0.60$
$\Omega_m$ . . . . .	$0.321 \pm 0.013$	$0.320 \pm 0.013$	$0.3166 \pm 0.0084$	$0.3158 \pm 0.0082$
$\Omega_\Lambda$ . . . . .	$0.679 \pm 0.013$	$0.680 \pm 0.013$	$0.6834 \pm 0.0084$	$0.6842 \pm 0.0082$
$\sigma_8$ . . . . .	$0.8118 \pm 0.0089$	$0.8155 \pm 0.0083$	$0.8120 \pm 0.0073$	$0.8154 \pm 0.0067$
$z_{re}$ . . . . .	$7.50 \pm 0.82$	$8.04 \pm 0.60$	$7.68 \pm 0.79$	$8.14 \pm 0.60$
$10^9 A_s$ . . . . .	$2.092 \pm 0.034$	$2.113 \pm 0.028$	$2.101^{+0.031}_{-0.034}$	$2.120 \pm 0.028$
$10^9 A_s e^{-2\tau}$ . . . . .	$1.884 \pm 0.014$	$1.884 \pm 0.014$	$1.884 \pm 0.012$	$1.884 \pm 0.012$
Age/Gyr . . . . .	$13.830 \pm 0.037$	$13.827 \pm 0.036$	$13.800 \pm 0.024$	$13.798 \pm 0.024$

source of uncertainty in CMB large scale polarization parameter estimation.

As explained in [Planck Collaboration V \(2019\)](#) (see in particular section 2.4) the level of T to P leakage in the *Planck* 2018 legacy release maps forced the *Planck* Collaboration to adopt a strategy for the large scale polarization likelihood entirely based on simulations. Furthermore the difficulty of building reliable covariance matrices leads to use a simulation based likelihood, built on the  $EE$  cross spectrum of 100 and 143 GHz. In the present analysis, we follow the same overall strategy, although the lower level of systematics could have allowed a semi-analytical approach (see e.g. [Mangilli et al. \(2015\)](#); [Vanneste et al. \(2018\)](#); [Hamimeche & Lewis \(2008\)](#); [Gerbin et al. \(2019\)](#)) which we leave to future analysis. With this method, we measure  $\tau = 0.0566^{+0.0053}_{-0.0062}$  at 68% C.L. when all the other  $\Lambda$ CDM parameter are kept fixed.

The main difference with respect to the *Planck* 2018 analysis (which yields  $\tau = 0.051 \pm 0.009$ ) is based on the correction of the second-order ADCNL effect presented in [Delouis et al. \(2019\)](#) which drastically reduces the dipole and foreground signals distortion allowing to recover almost completely  $\ell = 2$  and  $\ell = 3$  for the  $\tau$  determination, suppressed in previous analysis by a large variance (see e.g. [Planck Collaboration Int. XLVI \(2016\)](#); [Planck Collaboration V \(2019\)](#); [Planck Collaboration Int. XLVII \(2016\)](#)). As consequence of this in the SR0112  $EE$  100x143 spectrum the variance associated to systematics becomes smaller than the noise and cosmic variance making less critical the accuracy of the ADCNL simulation produced. Those aspects together with an improved version of the foreground model causes a  $\sim 1\text{-}\sigma$  upward shift in the  $\tau$  posterior.

In a more complete parameter exploration, combining the SR0112 likelihood with the temperature and high- $\ell$  polarization likelihood, we measure  $\tau = 0.059 \pm 0.006$  at 68% C.L. which represents the strongest constrain on the reionization optical depth

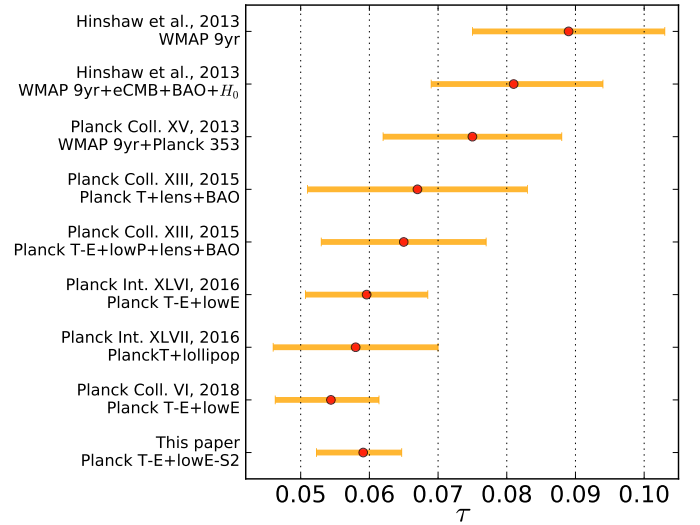


**Fig. 18.** History of  $\tau$  determination from WMAP to *Planck*. With *Planck* T tag we refer to *Planck* low- $\ell$  and high- $\ell$  temperature likelihood, with *Planck* T-E, we refer to low- $\ell$  and high- $\ell$  temperature likelihood combined with high- $\ell$   $TE$  and  $EE$  likelihood. WMAP 9yr + *Planck* 353 refers to the WMAP 9yr low- $\ell$  and high- $\ell$  likelihoods with the large scale polarization data cleaned by *Planck* 353GHz.

to date. The most recent optical depth measurement from CMB data in the context of  $\Lambda$ CDM model are reported in [Fig. 18](#).

Assuming instantaneous reionization, this corresponds to  $z_{re} = 8.14 \pm 0.61$  at 68% C.L. The tight bound on  $\tau$  breaks efficiently the  $A_s e^{-2\tau}$  degeneracy reducing the constraint on the fluctuation amplitude down to  $\sigma_8 = 0.8128 \pm 0.0053$  at 68% C.L..

The improvement with respect to *Planck* 2018 legacy release in the large scale polarization data leads to an expected reduction of the  $\tau$  uncertainty but it is matched with a slight shift upwards of the central value. This combination leads to a substantial unchanged  $\tau$  upper limit leaving to a mostly unchanged constraint on all the minimal  $\Lambda$ CDM extensions explored. Further investigations are left to future publications. The SRoll2 data maps, simulations and, likelihood code are publicly available at <http://sroll20.ias.u-psud.fr>.

**Acknowledgements.** We acknowledge the use of CAMB, HEALPix and Healpy software packages. This work is part of the Bware project, partially supported by CNES. It was granted access to the HPC resources of CINES (<http://www.cines.fr>) under the allocation 2017-A0030410267 made by GENCI (<http://www.genici.fr>). This research used resources of the National Energy Research Scientific Computing Center (NERSC), a U.S. Department of Energy Office of Science User Facility operated under Contract No. DE-AC02-05CH11231. LP is grateful to G. Fabbian, M. Lattanzi and M. Migliaccio for many helpful discussions during the preparation of this work. LP acknowledges the support of the National Centre for Space Studies (CNES) postdoctoral program and Italian Space Agency (ASI) grant 2016-24-H.0 (COSMOS).

## References

- Becker, R. H. et al., Evidence for Reionization at  $Z \approx 6$ : Detection of a Gunn-Peterson trough in a  $Z = 6.28$  Quasar. 2001, *Astron. J.*, 122, 2850, [arXiv:astro-ph/0108097](https://arxiv.org/abs/astro-ph/0108097)
- Benabed, K., Cardoso, J. F., Prunet, S., & Hivon, E., TEASING: a fast and accurate approximation for the low multipole likelihood of the Cosmic Microwave Background temperature. 2009, *Mon. Not. Roy. Astron. Soc.*, 400, 219, [arXiv:0901.4537](https://arxiv.org/abs/0901.4537)
- Bennett, C. L., Larson, D., Weiland, J. L., et al., Nine-year Wilkinson Microwave Anisotropy Probe (WMAP) Observations: Final Maps and Results. 2013, *ApJ Supp.*, 208, 20, [arXiv:1212.5225](https://arxiv.org/abs/1212.5225)
- Bouwens, R. J., Illingworth, G. D., Oesch, P. A., et al., Reionization after Planck: The Derived Growth of the Cosmic Ionizing Emissivity now matches the Growth of the Galaxy UV Luminosity Density. 2015, *Astrophys. J.*, 811, 140, [arXiv:1503.08228](https://arxiv.org/abs/1503.08228)
- Catalano, A., Coulais, A., & Lamarre, J.-M., Analytical approach to optimizing alternating current biasing of bolometers. 2010, *Appl. Opt.*, 49, 5938
- Dayal, P. & Ferrara, A., Early galaxy formation and its large-scale effects. 2018, *Phys. Rept.*, 780-782, 1, [arXiv:1809.09136](https://arxiv.org/abs/1809.09136)
- Delouis, J. M., Pagano, L., Mottet, S., Puget, J. L., & Vibert, L., SRoll2: an improved mapmaking approach to reduce large-scale systematic effects in the Planck High Frequency Instrument legacy maps. 2019, *Astron. Astrophys.*, 629, A38, [arXiv:1901.11386](https://arxiv.org/abs/1901.11386)
- Efstathiou, G., Hybrid estimation of cosmic microwave background polarization power spectra. 2006, *MNRAS*, 370, 343, [arXiv:astro-ph/0601107](https://arxiv.org/abs/astro-ph/0601107)
- Fan, X.-H., Strauss, M. A., Becker, R. H., et al., Constraining the evolution of the ionizing background and the epoch of reionization with  $z \approx 6$  quasars. 2. a sample of 19 quasars. 2006, *Astron. J.*, 132, 117, [arXiv:astro-ph/0512082](https://arxiv.org/abs/astro-ph/0512082)
- Finkbeiner, D. P., Davis, M., & Schlegel, D. J., Extrapolation of galactic dust emission at 100 microns to CMBR frequencies using FIRAS. 1999, *Astrophys. J.*, 524, 867, [arXiv:astro-ph/9905128](https://arxiv.org/abs/astro-ph/9905128)
- Gerbino, M., Lattanzi, M., Migliaccio, M., et al., Likelihood methods for CMB experiments. 2019, [arXiv:1909.09375](https://arxiv.org/abs/1909.09375)
- Górski, K. M., Hivon, E., Banday, A. J., et al., HEALPix: A Framework for High-Resolution Discretization and Fast Analysis of Data Distributed on the Sphere. 2005, *ApJ*, 622, 759, [arXiv:astro-ph/0409513](https://arxiv.org/abs/astro-ph/0409513)
- Gunn, J. E. & Peterson, B. A., On the Density of Neutral Hydrogen in Intergalactic Space. 1965, *Astrophys. J.*, 142, 1633
- Hamimeche, S. & Lewis, A., Likelihood Analysis of CMB Temperature and Polarization Power Spectra. 2008, *Phys. Rev.*, D77, 103013, [arXiv:0801.0554](https://arxiv.org/abs/0801.0554)
- Hinshaw, G., Larson, D., Komatsu, E., et al., Nine-year Wilkinson Microwave Anisotropy Probe (WMAP) Observations: Cosmological Parameter Results. 2013, *ApJ Supp.*, 208, 19, [arXiv:1212.5226](https://arxiv.org/abs/1212.5226)
- Hivon, E., Gorski, K. M., Netterfield, C. B., et al., Master of the cosmic microwave background anisotropy power spectrum: a fast method for statistical analysis of large and complex cosmic microwave background data sets. 2002, *Astrophys. J.*, 567, 2, [arXiv:astro-ph/0105302](https://arxiv.org/abs/astro-ph/0105302)
- Holmes, W. A., Bock, J. J., Crill, B. P., et al., Initial test results on bolometers for the Planck high frequency instrument. 2008, *Appl. Opt.*, 47, 5996
- Keskitalo, R., Ashdown, M. A. J., Cabella, P., et al., Residual noise covariance for Planck low-resolution data analysis. 2010, *A&A*, 522, A94, [arXiv:0906.0175](https://arxiv.org/abs/0906.0175)
- Kogut, A., Spergel, D. N., Barnes, C., et al., First-Year Wilkinson Microwave Anisotropy Probe (WMAP) Observations: Temperature-Polarization Correlation. 2003, *ApJ Supp.*, 148, 161, [arXiv:astro-ph/0302213](https://arxiv.org/abs/astro-ph/0302213)
- Lattanzi, M., Burigana, C., Gerbino, M., et al., On the impact of large angle CMB polarization data on cosmological parameters. 2017, *JCAP*, 1702, 041, [arXiv:1611.01123](https://arxiv.org/abs/1611.01123)
- Lewis, A. & Bridle, S., Cosmological parameters from CMB and other data: A Monte Carlo approach. 2002, *Phys. Rev. D*, 66, 103511, [arXiv:astro-ph/0205436](https://arxiv.org/abs/astro-ph/0205436)
- Lewis, A., Challinor, A., & Lasenby, A., Efficient computation of CMB anisotropies in closed FRW models. 2000, *ApJ*, 538, 473, [arXiv:astro-ph/9911177](https://arxiv.org/abs/astro-ph/9911177)
- Mangilli, A., Plaszczyński, S., & Tristram, M., Large-scale cosmic microwave background temperature and polarization cross-spectra likelihoods. 2015, *Mon. Not. Roy. Astron. Soc.*, 453, 3174, [arXiv:1503.01347](https://arxiv.org/abs/1503.01347)
- Page, L., Hinshaw, G., Komatsu, E., et al., Three-Year Wilkinson Microwave Anisotropy Probe (WMAP) Observations: Polarization Analysis. 2007, *ApJ Supp.*, 170, 335, [arXiv:astro-ph/0603450](https://arxiv.org/abs/astro-ph/0603450)
- Pajot, F., Ade, P. A. R., Beney, J., et al., *Planck* pre-launch status: HFI ground calibration. 2010, *A&A*, 520, A10
- Planck Collaboration ES. 2013, The Explanatory Supplement to the *Planck* 2013 results, <https://www.cosmos.esa.int/web/planck/pla> (ESA)
- Planck Collaboration ES. 2015, The Explanatory Supplement to the *Planck* 2015 results, <https://www.cosmos.esa.int/web/planck/pla> (ESA)
- Planck Collaboration ES. 2018, The Legacy Explanatory Supplement, <https://www.cosmos.esa.int/web/planck/pla> (ESA)
- Planck Collaboration XV, *Planck* 2013 results. XV. CMB power spectra and likelihood. 2014, *A&A*, 571, A15, [arXiv:1303.5075](https://arxiv.org/abs/1303.5075)
- Planck Collaboration XVI, *Planck* 2013 results. XVI. Cosmological parameters. 2014, *A&A*, 571, A16, [arXiv:1303.5076](https://arxiv.org/abs/1303.5076)
- Planck Collaboration VIII, *Planck* 2015 results. VIII. High Frequency Instrument data processing: Calibration and maps. 2016, *A&A*, 594, A8, [arXiv:1502.01587](https://arxiv.org/abs/1502.01587)
- Planck Collaboration XI, *Planck* 2015 results. XI. CMB power spectra, likelihoods, and robustness of parameters. 2016, *A&A*, 594, A11, [arXiv:1507.02704](https://arxiv.org/abs/1507.02704)
- Planck Collaboration XII, *Planck* 2015 results. XII. Full Focal Plane simulations. 2016, *A&A*, 594, A12, [arXiv:1509.06348](https://arxiv.org/abs/1509.06348)
- Planck Collaboration XIII, *Planck* 2015 results. XIII. Cosmological parameters. 2016, *A&A*, 594, A13, [arXiv:1502.01589](https://arxiv.org/abs/1502.01589)
- Planck Collaboration II, *Planck* 2018 results. II. Low Frequency Instrument data processing. 2019, *A&A*, in press, [arXiv:1807.06206](https://arxiv.org/abs/1807.06206)
- Planck Collaboration III, *Planck* 2018 results. III. High Frequency Instrument data processing. 2019, *A&A*, in press, [arXiv:1807.06207](https://arxiv.org/abs/1807.06207)
- Planck Collaboration IV, *Planck* 2018 results. IV. Diffuse component separation. 2019, *A&A*, in press, [arXiv:1807.06208](https://arxiv.org/abs/1807.06208)
- Planck Collaboration V, *Planck* 2018 results. V. Power spectra and likelihoods. 2019, *A&A*, submitted, [arXiv:1907.12875](https://arxiv.org/abs/1907.12875)
- Planck Collaboration VI, *Planck* 2018 results. VI. Cosmological parameters. 2019, *A&A*, submitted, [arXiv:1807.06209](https://arxiv.org/abs/1807.06209)
- Planck Collaboration VIII, *Planck* 2018 results. VIII. Gravitational lensing. 2019, *A&A*, in press, [arXiv:1807.06210](https://arxiv.org/abs/1807.06210)
- Planck Collaboration Int. XLVI, *Planck* intermediate results. XLVI. Reduction of large-scale systematic effects in HFI polarization maps and estimation of the reionization optical depth. 2016, *A&A*, 596, A107, [arXiv:1605.02985](https://arxiv.org/abs/1605.02985)
- Planck Collaboration Int. XLVII, *Planck* intermediate results. XLVII. Constraints on reionization history. 2016, *A&A*, 596, A108, [arXiv:1605.03507](https://arxiv.org/abs/1605.03507)
- Planck Collaboration Int. LI, *Planck* intermediate results. LI. Features in the cosmic microwave background temperature power spectrum and shifts in cosmological parameters. 2017, *A&A*, 607, A95, [arXiv:1608.02487](https://arxiv.org/abs/1608.02487)
- Rauch, M., The Lyman alpha forest in the spectra of quasistellar objects. 1998, *Ann. Rev. Astron. Astrophys.*, 36, 267, [arXiv:astro-ph/9806286](https://arxiv.org/abs/astro-ph/9806286)
- Scheuer, P. A. G., A Sensitive Test for the Presence of Atomic Hydrogen in Intergalactic Space. 1965, *Nature*, 207, 963
- Tegmark, M., A method for extracting maximum resolution power spectra from microwave sky maps. 1996, *MNRAS*, 280, 299, [arXiv:astro-ph/9412064](https://arxiv.org/abs/astro-ph/9412064)
- Tegmark, M. & de Oliveira-Costa, A., How to measure CMB polarization power spectra without losing information. 2001, *Phys. Rev.*, D64, 063001, [arXiv:astro-ph/0012120](https://arxiv.org/abs/astro-ph/0012120)
- Tristram, M., Macias-Perez, J. F., Renault, C., & Santos, D., Xspectrum, estimation of the angular power spectrum by computing cross power spectra. 2005, *Mon. Not. Roy. Astron. Soc.*, 358, 833, [arXiv:astro-ph/0405575](https://arxiv.org/abs/astro-ph/0405575)
- Vanneste, S., Henrot-Versill, S., Louis, T., & Tristram, M., Quadratic estimator for CMB cross-correlation. 2018, *Phys. Rev.*, D98, 103526, [arXiv:1807.02484](https://arxiv.org/abs/1807.02484)

Weiland, J. L., Osumi, K., Addison, G. E., et al., Effect of Template Uncertainties on the WMAP and Planck Measures of the Optical Depth Due To Reionization. 2018, *Astrophys. J.*, 863, 161, [arXiv:1801.01226](#)